Open access • Journal Article • DOI:10.1007/S11071-008-9463-Y

Simulation and stability analysis of impacting systems with complete chattering

Arne Nordmark, Petri T. Piiroinen

Institutions: Royal Institute of Technology, National University of Ireland, Galway

Published on: 09 Jan 2009 - Nonlinear Dynamics (Springer Netherlands)

Topics: Dynamical systems theory

Simulation and stability analysis of impacting systems with complete chattering

Arne Nordmark, Petri Piiroinen

Simulation and stability analysis of impacting systems with complete chattering

Arne B. Nordmark, **Petri T. Piiroinen**

Abstract This paper considers dynamical systems that are derived from mechanical systems with impacts. In particular we will focus on chattering—accumulation of impacts—for which local discontinuity mappings will be derived. We will first show how to use these mappings in simulation schemes, and secondly how the mappings are used to calculate the stability of limit cycles with chattering by solving the first variational equations.

Keywords
Nonlinear dynamics
Impacting systems
Chattering
Stability analysis
Bifurcations
Discontinuity mappings
Numerical methods
Simulation

1 Introduction

Impacts can be found in many (bio-)mechanical systems. Sometimes they are desirable and necessary, such as in two-legged walking [32], church bells [3] and Braille printers [8, 19]. However, very often impacts are unwanted and cause unexpected wear and noise, such as in gears [18] and cam-follower systems [28]. There has been research into developing theoretical impact models [4, 17, 31, 36], as well as, using numerical simulations [29, 30, 35] and experiments [16, 37], to understand impacts from both microscopical and global perspectives. Despite all this effort no ultimate impact model has been presented and is still to be discovered. Luckily, simple impact models, such as Newton's impact law, work remarkably well in many situation and are therefore used in many applications. The advantage of these simple impact models is that they can be easily combined with the standard framework for deriving equations of motion of mechanical systems, i.e. as systems of second-order ordinary differential equations (ODEs). For analysis purposes such systems are often transformed to first-order ODEs and thus results from dynamical system theory can be applied. This will be the foundation for the work in the present paper.

Impacting systems are often put into a larger class of systems called *non-smooth* (NS) or *piecewise smooth* (PWS) systems. A common feature for most of these systems is that they are smooth, or even linear, away from *discontinuity surfaces* but at the surfaces something that causes nonlinearities occurs, such as impacts. Another important feature is that these systems often have dynamical characteristics that can-

not be found in smooth systems. For instance, interaction of equilibria or limit cycles with a discontinuity surface can lead to instantaneous changes in stability, which cannot be experienced in smooth systems. All such interactions we collectively term *discontinuity-induced bifurcations* (DIBs), but they are also sometimes known as *C-bifurcations* or *border-collision bifurcations* [13, 14, 20]. The type of DIB is heavily dependent on the type of NS systems in question, and therefore there is a substantial terminology detailing what kind of DIB that is studied, e.g. *grazing bifurcations* in impacting systems [22–24], *sliding bifurcations* in electrical [7, 10, 11] and mechanical systems with dry friction [12, 34], and *corner bifurcations* [6]. Since some DIBs do not have center manifolds in the classical sense, and thus cannot be used to unfold the dynamics locally, the concept of *discontinuity mappings* (DMs) [23, 25] have instead been introduced as a useful tool to unfold the dynamics at DIBs. In recent years DMs have been used to unfold codimension-one and codimension-two DIBs in a variety of systems and situations [12, 27].

A special feature of impacting systems, and the main topic of this article, is the possibility of *chattering* [5]. We will distinguish between two different types of chattering, namely, *complete* and *incomplete* chattering. Complete chattering refers to the phenomenon where a system undergoes an *infinite* number of impacts in a finite time, where the impact velocity goes uniformly to zero. Incomplete chattering refers to a sequence of impacts that initially has the same behavior as complete chattering but that ends after a large but *finite* number of impacts. In Figs. 1(a) and (b) we show a time series of the position and velocity, respectively, for a vertically moving ball under the influence gravity bouncing against a rigid surface that undergoes complete chattering. It is notable that chattering as defined here is sometimes also referred to as *Zeno phenomenon* [38], and that the term chattering is sometimes used in control theory to refer to a large number of switches, and in mechanical engineering to a large number of recurrent impacts, not necessarily infinite.

When faced with a new NS dynamical system, the first and most straightforward way of analyzing the dynamics is to perform a direct numerical simulation (DNS) of the system, i.e. to solve an initial value problem (IVP). In some special cases one might be able to find the analytic solution to the ODE, but generally one needs to solve a system of ODEs numerically. There are many different numerical solvers for smooth systems [1, 33], but the question is how to deal with interactions between solutions and discontinuity surfaces. There are a number of different strategies of which the two mostly used are the *time-stepping* and *event-driven* strategies. Ultimately both methods are time steppers, but in the first case there is a check if a discontinuity surface has been crossed at each time step, and if that is the case the ODE is adjusted, e.g. by applying an impulsive force at an impact. In the second case there is also a check if a discontinuity surface has been crossed at each time step, but when such a crossing is detected the point of penetration will be more precisely located, with an *event-location routine*, from which point the simulation continues and the system is adjusted. The adjustment could be through an impulsive force, as above, or a discrete map. The method of solving a combination of smooth systems and discrete maps is sometimes termed a *hybrid-system* approach. In the hybrid-system approach the simulation is stopped when the event has been located and a discrete map is applied to the state and/or the system of ODEs are replaced. Here we will use this last strategy for simulation of impacting systems, which means that

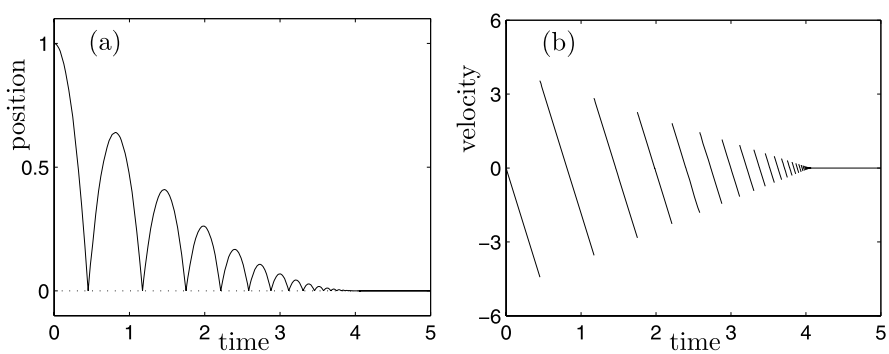

Fig. 1 The (**a**) position and (**b**) velocity versus time of a bouncing ball, with coefficient of restitution $e = 0.8$, that undergoes a complete chattering sequence

we can use a high-order ODE solver between events and focus more on how to deal with the discontinuous elements. Another advantage with this strategy is that it is relatively straightforward to calculate the stability of limit cycles by solving the *first variational equations*, using *saltation matrices* [21], and ultimately to continue them under parameter variation [2]. Unlike boundary value solver software like AUTO [15] and SLIDECONT [9], that are based on *collocation*, where the entire event order has to be predescribed, hybrid-system based software uses *shooting* and does not require a predescribed event order, but all necessary quantities are calculated during simulation.

The focus of this article is threefold. Firstly, we will show how to simulate impacting systems that undergo complete chattering by deriving the necessary mapping to bypass the tail of the complete chattering (see [5] for related work). We will also give a detailed description of our proposed numerical algorithm for simulation of impacting systems with chattering. Secondly, we will show what measures need to be taken in order to calculate the stability of a trajectory with chattering and thus how it can be used to locate and continue periodic orbits. Thirdly, we will introduce an example to show that our proposed numerical method works in three different cases.

The remainder of the present article is organized as follows. Section 2 introduces and defines concepts needed for the treatment of impacting systems, such as the impacting surface, the impact law, sticking and chattering. In Sect. 3 the local map that bypasses the tail of a complete chattering sequence is derived and explained. Section 4 describes how to calculate the stability of a limit cycle with chattering and also discusses how the numerical robustness can be improved. In Sect. 5 the numerical scheme we propose for simulation is explained and in Sect. 6 we apply the simulation and analysis methods to a mechanical system, a forced double pendulum. Finally, in Sect. 7 we conclude the article.

2 Impacting systems

We will here introduce a rather general model for an impacting system described by a smooth vector field (F) and impacting on a smooth surface (S_0^0) in state space. Impacts are taken to cause an instantaneous change in the system state (i.e. an impact takes zero time), and we use a *restitution law* to describe the state change (cf. Newton's impact law). The reason for considering only one impact surface is that the main topic of this paper, chattering, is a local phenomenon involving only one impact surface, and also that a simultaneous impact at two different surfaces may involve the simultaneous application of two incompatible impact laws, and solutions that are not unique in forward time (see [6]). The components of our model are a vector field F, a scalar function H whose zero level set describes the impact surface, and a function W used in the impact law. We will assume that these three functions are analytic.

2.1 The vector field

Let S be a subset of $\mathbb{R}^n$ and let F be a vector field on S with a corresponding system of ODEs given by

$$\dot{x} = F(x), \quad x \in S \subset \mathbb{R}^n.$$

Since we would like to have solutions for all forward times, let us assume that trajectories of the vector field do not reach the boundary of S in finite time. Thus the vector field defines an analytic flow function $\phi : S \times \mathbb{R} \mapsto S$ so that

$$\phi_t(x,t) = F\big(\phi(x,t)\big), \quad \phi(x,0) = x. \tag{1}$$

Notice that will often use subscripts '$_x$' and '$_t$' to denote partial derivatives.

2.2 The impact surface

Let the impact surface (S_0^0) be given by the zero level set of a scalar function $H : S \mapsto \mathbb{R}$, which has non-zero gradient on this level set, and that the system should be constrained to those points of S where $H \geq 0$. Define the *Lie derivative* $\mathcal{L}_F(H)$ of H along F so that

$$\mathcal{L}_F(H)(x) := H_t\big(\phi(x,t)\big)\big|_{t=0} = H_x(x)F(x)$$

and inductively

$$\mathcal{L}_F^0(H) = H, \qquad \mathcal{L}_F^k(H) = \mathcal{L}_F\big(\mathcal{L}_F^{k-1}(H)\big).$$

In particular we denote the velocity relative to H by

$$v(x) := \mathcal{L}_F(H)(x) \tag{2}$$

and the acceleration by

$$a(x) := \mathcal{L}_F^2(H)(x). \tag{3}$$

For future reference we also define some useful subsets of S:

$$S_k^+ := \big\{x \in S \mid \mathcal{L}_F^k(H)(x) > 0\big\},$$
$$S_k^0 := \big\{x \in S \mid \mathcal{L}_F^k(H)(x) = 0\big\},$$
$$S_k^- := \big\{x \in S \mid \mathcal{L}_F^k(H)(x) < 0\big\},$$
$$\Sigma_k^+ := \left(\bigcap_{m=0}^{k-1} S_m^0\right) \cap S_k^+, \qquad \Sigma_k^0 := \left(\bigcap_{m=0}^{k-1} S_m^0\right) \cap S_k^0,$$
$$\Sigma_k^- := \left(\bigcap_{m=0}^{k-1} S_m^0\right) \cap S_k^-$$

for non-negative integers k. This means that each zero set Σ_k^0 is further divided into subsets through

$$\Sigma_k^0 = \Sigma_{k+1}^+ \cup \Sigma_{k+1}^0 \cup \Sigma_{k+1}^-.$$

Thus, the desired region for the system is $\Sigma_0^+ \cup \Sigma_0^0$. However, at points in $\bigcup_{m=1}^{\infty} \Sigma_m^-$ the system would leave this region. We have to introduce an impact law and sticking motion to be able to continue from these points.

2.2.1 *Example: a periodically forced 1DOF linear oscillator*

Consider the ODE

$$\ddot{q} + 2\zeta\dot{q} + q = \cos(\omega t), \quad q \geq \sigma.$$

Letting $x = (x_1, x_2, x_3)^{\mathrm{T}}$, where $x_1 = q$, $x_2 = \dot{q}$ and $x_3 = \omega t \pmod{2\pi}$, we can take $S = \mathbb{R}^n$, use the vector field

$$F(x) = \begin{pmatrix} x_2 \\ -x_1 - 2\zeta x_2 + \cos(x_3) \\ \omega \end{pmatrix} \tag{4}$$

and $H(x) = x_1 - \sigma$ as the scalar function defining the impacting surface. The velocity and acceleration relative to H becomes

$$v(x) = x_2 \quad \text{and} \quad a(x) = -x_1 - 2\zeta x_2 + \cos(x_3),$$

respectively. We also have

$$\Sigma_0^+ = \{x \mid x_1 > \sigma\}, \qquad \Sigma_1^+ = \{x \mid x_1 = \sigma, x_2 > 0\},$$
$$\Sigma_1^- = \{x \mid x_1 = \sigma, x_2 < 0\}$$

and if for example $\sigma = 0$ and $\omega > 0$, we have

$$\Sigma_2^+ = \big\{x \mid x_1 = 0,\ x_2 = 0,\ x_3 \in [0, \pi/2) \cup (3\pi/2, 2\pi)\big\},$$
$$\Sigma_2^- = \big\{x \mid x_1 = 0,\ x_2 = 0,\ x_3 \in (\pi/2, 3\pi/2)\big\},$$
$$\Sigma_3^+ = \left\{\begin{pmatrix} 0 \\ 0 \\ 3\pi/2 \end{pmatrix}\right\}, \qquad \Sigma_3^- = \left\{\begin{pmatrix} 0 \\ 0 \\ \pi/2 \end{pmatrix}\right\},$$

and the union of these disjoint sets is precisely those points x where $H(x) \geq 0$. These sets are shown in Fig. 2.

2.3 The impact law

First consider a point $x \in \Sigma_1^-$ where $H(x) = 0$ and the velocity $v(x) < 0$. We now need an impact law $\tilde{R}(x)$ defined on S_0^0 that gives a new state with $H(\tilde{R}(x)) = 0$ and $v(\tilde{R}(x)) \geq 0$. We will further assume that the mapping reduces to identity (no state jump) as the impact velocity approaches zero, and that $\tilde{R}$ can be extended to an analytic mapping $R : S \mapsto S$. The condition that $v = 0$ should lead to no-jump means that R must have the form

$$R(x) = x + W(x)v(x) \tag{5}$$

for some analytic function $W : S \mapsto \mathbb{R}^n$. The function W is further restricted by the condition

$$R(\Sigma_1^-) \subset \big(\Sigma_1^+ \cup \Sigma_1^0\big). \tag{6}$$

Substituting (5) into (2) to compute the new velocity gives

$$\begin{aligned} &v\big(x + W(x)v(x)\big) \\ &\quad = v(x) + \nabla v(x) W(x) v(x) + \mathcal{O}\big(v(x)\big)^2 \\ &\quad = \big(1 + \mathcal{L}_W\big(\mathcal{L}_F(H)\big)(x)\big)v(x) + \mathcal{O}\big(v(x)\big)^2 \end{aligned} \tag{7}$$

and thus we can identify a low-velocity "coefficient of restitution" as

$$r(x) = -\big(1 + \mathcal{L}_W \mathcal{L}_F(H)(x)\big). \tag{8}$$

From (6) we must have

$$0 \leq r(x) \tag{9}$$

at a point $x \in \Sigma_1^0$.

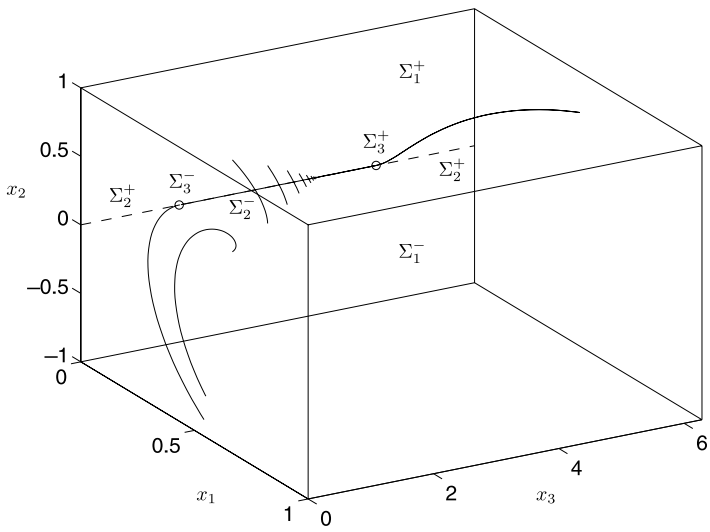

Fig. 2 The Σ sets and two sticking trajectories for the periodically forced 1DOF linear impact oscillator. Parameter values are $\zeta = 0.1$, $\omega = 1$, $\sigma = 0$, and the restitution coefficient $e = 0.6$. One trajectory enters sticking without impact through Σ_3^-. The other enters sticking through a complete chattering sequence. Both orbits coincide after exiting from sticking, which happens at Σ_3^+. Notice that $x_3 = \omega t$ (see (4))

The appearance of something like a coefficient of restitution here is just a consequence of the jump map being assumed to be analytic and that it should reduce to no-jump in the case of zero normal velocity.

If $x \in \bigcup_{m=2}^{\infty} \Sigma_m^-$, where $v(x) = 0$, then the impact law does nothing but we still have to prevent the system from leaving the allowed region, which is dealt with next.

2.4 Sticking

Suppose now that $x \in \bigcup_{m=2}^{\infty} \Sigma_m^-$. The process that keeps the system constrained to Σ_0^0 during an infinitesimal time interval dt can be viewed as a combination of the action of the vector field F and of "impacting with an infinitesimally small negative velocity du" which gives $dx = F(x)\,dt - |du|W(x)$. We call this process *sticking* (or *sliding*, in some circumstances). Thus, the sticking vector field is given by

$$\dot{x} = F'(x) = F(x) - \lambda(x)W(x), \quad \lambda \geq 0, \tag{10}$$

where λ must be chosen to keep the system in Σ_1^0 (λ is essentially a Lagrange multiplier for the constrained system). Since the jump map R maps the impact surface Σ_0^0 back to itself, we must have that W is tangent to Σ_0^0 when $x \in \Sigma_1^0$, which means that $x \in \Sigma_1^0 \Rightarrow \mathcal{L}_W(H)(x) = 0$.

Then we can show that the sticking vector field F' is automatically tangent to Σ_0^0 since

$$\mathcal{L}_{F'}(H)(x) = \mathcal{L}_F(H)(x) - \lambda(x)\mathcal{L}_W(H)(x) = 0 \tag{11}$$

for any $\lambda(x)$ when $x \in \Sigma_1^0$. Since the sticking vector field should also be tangent to Σ_1^0, we want

$$\begin{aligned}\mathcal{L}_{F'}(v)(x) &= \mathcal{L}_{F'}\mathcal{L}_F(H)(x) \\ &= \mathcal{L}_F^2(H)(x) - \lambda(x)\mathcal{L}_W\mathcal{L}_F(H)(x) = 0\end{aligned}$$

which gives

$$\lambda(x) = \frac{\mathcal{L}_F^2(H)(x)}{\mathcal{L}_W\mathcal{L}_F(H)(x)} = \frac{-a(x)}{1 + r(x)}. \tag{12}$$

Since $0 \leq r(x)$ when $x \in \Sigma_1^0$ (by (9)), we see that $\lambda(x)$ is well defined there, $F'(x)$ is tangent to Σ_1^0, and if $a(x) \leq 0$ then $\lambda(x)$ is non-negative. The sticking phase ends when $x \in \bigcup_{m=3}^{\infty} \Sigma_m^+$.

A trajectory of F can only enter the sticking set, without impacts, at points in Σ_m^- for some odd $m \geq 3$, which is a subset of the impact surface Σ_0^0 of at least codimension-two (see the leftmost trajectory in Fig. 2). Thus the direct transition from free flight to sticking is rather unlikely. Another possibility is that the impact map R maps a point in Σ_1^- to a point in Σ_1^0 (with zero outgoing velocity) through a "completely inelastic" impact, which happens only in a rather special class of impacting systems, i.e. when $r(x) = 0$. The typical way of entering sticking is instead through an accumulation of impacts with lower and lower velocities, i.e. chattering.

2.5 Chattering

It may happen that an infinite number of impacts accumulate in finite time. Since the time between impacts

goes to zero, the same must happen with the velocity, and the accumulation point x must lie in $\Sigma_2^- \cup \Sigma_2^0$ where $H(x) = 0$, $v(x) = 0$, $a(x) \le 0$. For example, if $a(x) < 0$, $0 < r(x) < 1$, and $H(x)$, $v(x)$ are small enough, then impacts will accumulate at a point in Σ_2^- near x. This typical situation will be our focus in the rest of the paper.

2.5.1 *Example continued: a periodically forced 1DOF linear impact oscillator*

We complete the example of Sect. 2.2.1 by specifying that when q reaches σ with negative velocity $\dot{q}^-$, an impact should occur such that

$$\dot{q}^+ = -e\dot{q}^- \quad \text{when } q = \sigma \quad \text{and} \quad \dot{q}^- < 0,$$

where e correspond to a Newton coefficient of restitution. Using the state x as defined above, we find that the impact function W becomes

$$W(x) = \begin{pmatrix} 0 \\ -(1+e) \\ 0 \end{pmatrix} \quad \text{so that}$$

$$R(x) = x + \begin{pmatrix} 0 \\ -(1+e) \\ 0 \end{pmatrix} x_2,$$

and $r(x)$ as defined by (8) is equal to e, as expected. In Fig. 2 two trajectories with a sticking section are shown. One is the special trajectory that enters sticking without impact, and the second nearby one is a more typical trajectory that enters sticking through a complete chattering sequence. Both trajectories leave the sticking set at the same point.

3 The chatter mapping

Our goal in this section is to show that if $\bar{x}$ is a point in Σ_2^- and $0 \le r(\bar{x}) < 1$, then for all points $x \in \Sigma_1^- \cup \Sigma_2^-$ close to $\bar{x}$ there is a unique point $x^* = Q(x)$ and a unique time interval $\Delta t^* = q(x)$ where chatter completes. Furthermore, the mappings Q and q are smooth.

First, if $x \in \Sigma_2^-$, then we can take $x^* = Q(x) = x$ and $\Delta t^* = q(x) = 0$. Thus we may assume that $x \in \Sigma_1^-$. A point in Σ_1^- will immediately undergo an impact, and then a short trajectory of F will bring us back to Σ_1^- again. This gives a "next impact" mapping, and applying this mapping an infinite number of times should lead us to the point x^*, where chatter completes. This point x^* is also a fixed point of the mapping, and x belongs to the stable manifold of x^*.

3.1 The generalized next impact mapping

The mappings $Q(x)$ and $q(x)$ reduce to the identity and zero, respectively, whenever $v(x) = 0$. We can take advantage of this by introducing an auxiliary variable v to track the velocity $v(x) = \mathcal{L}_F(H)(x)$, independently of the state x. The goal is to be able to write the mappings as power series in the scalar variable v, with coefficients that are known functions of x, instead of having to expand in the non-scalar state variable x. Thus we will derive *generalized mappings* depending on x and v, which will reduce to the correct mappings depending on x only when we set $v = \mathcal{L}_F(H)(x)$. To achieve the goal of having a power series in v, we will be adding terms that evaluate to 0 to the equations defining the mappings. For several examples of the same type of techniques, see Chaps. 6–8 in [14].

Thus, in the following, we will use v as an auxiliary variable independent of x, keeping in mind that in the final result we will let $v = \mathcal{L}_F(H)(x)$. We will always take x in a neighborhood of Σ_2^-, and v small.

3.1.1 *Impact*

The first thing that happens to a point in Σ_1^- is the impact, given by the jump map R. Let us view the impact velocity v as being independent of x and define

$$X_1(x, v) = x + W(x)v, \tag{13}$$

$$V_1(x, v) = \mathcal{L}_F(H)\big(X_1(x, v)\big) - \mathcal{L}_F(H)(x) + v \tag{14}$$

(rather than $X_1(x) = R(x)$, $V_1(x) = \mathcal{L}_F(H)(R(x))$). Note that if $v = \mathcal{L}_F(H)(x)$ then

$$X_1\big(x, \mathcal{L}_F(H)(x)\big) = R(x), \tag{15}$$

$$V_1\big(x, \mathcal{L}_F(H)(x)\big) = \mathcal{L}_F(H)\big(R(x)\big), \tag{16}$$

so X_1 is the jump map and V_1 is the outgoing velocity. On the other hand, for all x and small v, the linearization around $v = 0$ is

$$X_1(x, v) = x + W(x)v, \tag{17}$$

$$V_1(x, v) = -r(x)v + \mathcal{O}\big(v^2\big), \tag{18}$$

as was established in (7). Note again that without writing equations (13–14) this way, V_1 would not have had a vanishing zeroth-order term in the v power series expansion.

3.1.2 Flow to next impact

The second thing that happens is that a trajectory leads to the next impact. If we start with $H(x) = 0$, $v(x) > 0$ small, $a(x) < 0$, then the trajectory intersects Σ_1^- after a time that is proportional to $v(x)$ to lowest order. With this in mind we define the function $T_2(x, v)$ implicitly as the solution of

$$\begin{aligned} E_2(x, v, T_2) &= \frac{H(\phi(x, T_2)) - H(x)}{T_2} \\ &\quad - \mathcal{L}_F(H)(x) + v = 0, \\ T_2(x, 0) &= 0, \end{aligned} \tag{19}$$

where ϕ is the flow of F defined by (1). Note that since $a(x) \neq 0$ and

$$E_2(x, v, t) = v + ta(x)/2 + \mathcal{O}\big(t^2\big),$$

the implicit function theorem applies. Also note that if $H(x) = 0$ and $v = \mathcal{L}_F(H)(x)$, then $H(\phi(x, T_2(x, \mathcal{L}_F(H)(x))) = 0$, so T_2 is the time to next impact. Note again that trying to write (19) simply as $H(\phi(x, T_2)) = 0$, would neither have allowed us to use the implicit function theorem, since the Jacobian with respect to T_2 is always 0 at the x points of interest, nor would it have allowed us to write the flight time as a power series in v with a vanishing zeroth order term.

Now define

$$X_2(x, v) = \phi\big(x, T_2(x, v)\big) = x - \frac{2F(x)}{a(x)}v + \mathcal{O}\big(v^2\big), \tag{20}$$

$$\begin{aligned} V_2(x, v) &= \mathcal{L}_F(H)\big(X_2(x, v)\big) - \mathcal{L}_F(H)(x) + v \\ &= -v + \mathcal{O}\big(v^2\big). \end{aligned} \tag{21}$$

Again, if $H(x) = 0$ and $v = \mathcal{L}_F(H)(x)$ then X_2 is the point of next impact and V_2 is the impact velocity, but they are well-defined functions for all small v and all x where $a(x) < 0$.

3.2 Fixed points

We now define the generalized next impact mapping when $a(x) < 0$ and v small as

$$\begin{aligned} X_3(x, v) &= X_2\big(X_1(x, v), V_1(x, v)\big) \\ &= x + K(x)v + \mathcal{O}\big(v^2\big), \end{aligned} \tag{22}$$

$$V_3(x, v) = V_2\big(X_1(x, v), V_1(x, v)\big) = r(x)v + \mathcal{O}\big(v^2\big), \tag{23}$$

where

$$K(x) = \frac{2F(x)}{a(x)}r(x) + W(x). \tag{24}$$

For any $M < 0$, define the set

$$D = \big\{(x, v) \in \mathbb{R}^n \times \mathbb{R} \mid a(x) \leq M < 0, v = 0\big\}.$$

Then the generalized next impact mapping defines a dynamical system in a neighborhood of D, and each point in D is a fixed point. The Jacobian of the mapping evaluated at the fixed point is

$$J(x) = \begin{pmatrix} I & K(x) \\ 0 & r(x) \end{pmatrix} \tag{25}$$

where I is the $n \times n$ identity matrix. Clearly this matrix has n eigenvalues equal to 1, corresponding to the n-dimensional manifold of fixed points D, and one non-trivial eigenvalue $r(x)$. If $0 \leq r(x) < 1$ this eigenvalue lies inside the unit circle in the complex plane and hence the linearized map is stable. The corresponding stable (right) eigenvector is

$$\begin{pmatrix} \theta(x) \\ 1 \end{pmatrix} = \begin{pmatrix} -\frac{K(x)}{1-r(x)} \\ 1 \end{pmatrix}. \tag{26}$$

Furthermore, if the linearized map is stable, there are no other fixed points nearby with $v \neq 0$ and small.

3.3 Stable manifold

The stable manifold theorem now tells us that there exists a unique one-dimensional stable manifold

$$x = X_4(x^*, v) = x^* + \theta(x^*)v + \mathcal{O}\big(v^2\big) \tag{27}$$

through each fixed point $(x^*, 0) \in D$ that solves the equation

$$X_3\big(X_4(x, v), v\big) = X_4\big(x, V_3(X_4(x, v), v)\big). \tag{28}$$

Since D itself is n-dimensional, the union of the stable manifolds fills out an open subset of $\mathbb{R}^n \times \mathbb{R}$. If we for a given x can find a point x^* such that

$$x = X_4\big(x^*, \mathcal{L}_F(H)(x)\big),$$

then x^* is the point where chatter completes. To see that this is always possible, we invoke the implicit function theorem again. Let $X_5(x, v)$ solve

$$\begin{aligned} E_5(x, v, X_5) &= X_4(X_5, v) - x \\ X_5(x, 0) &= x. \end{aligned} \tag{29}$$

This gives $X_5(x, v) = x - \theta(x)v + \mathcal{O}(v^2)$, where θ is given by (26).

Our result can now finally be stated: If $H(x) = 0$, $v(x) < 0$ and small enough, $a(x) < 0$, and $0 \leq r(x) < 1$, then the dynamics starting at x leads to chattering that completes at

$$\begin{aligned} x^* &= Q(x) = X_5\big(x, v(x)\big) \\ &= x + \frac{1}{1 - r(x)}\left(\frac{2F(x)}{a(x)}r(x) + W(x)\right)v(x) \\ &\quad + v(x)^2\mathcal{O}(1) \end{aligned} \tag{30}$$

(where $\mathcal{O}(1)$ indicates a bounded function of x). The function $X_5(x, v)$ can be computed as a power series in v to any order (assuming F, H, W to be sufficiently smooth) by using the implicit function and stable manifold theorems.

Equation (30) can also be used to compute the time it takes for chatter to complete (we can include a new variable tracking the flow of time in the system by extending F with an extra component equal to 1 and W with 0). The result is

$$\begin{aligned} \Delta t^* &= q(x) \\ &= \frac{1}{1 - r(x)}\left(\frac{2}{a(x)}r(x)\right)v(x) + v(x)^2\mathcal{O}(1). \end{aligned} \tag{31}$$

Maps like these have been derived for particular systems before, for example in [5].

3.4 Estimating the truncation error

The map derived in Sect. 3.3 will naturally introduce a truncation error, and in what follows we will estimate this error.

Let $X_5^{(k)}(x, v)$ be the truncation of X_5 to order k in v. Thus $X_5^{(0)}(x, v) = x$ and $X_5^{(k+1)}(x, v) = X_5^{(k)}(x, v) + C_{k+1}(x)v^{k+1}$ for some coefficients $C_i(x)$. For small v, the error in using $X_5^{(n)}$ instead of X_5 will be dominated by the first neglected term $C_{n+1}(x)v^{k+1}$.

Equations (28)–(29) imply that

$$X_5\big(X_3(x, v), V_3(x, v)\big) - X_5(x, v) = 0 \tag{32}$$

(which may in fact be used together with $X_5(x, 0) = x$ to compute X_5 directly without having to compute X_4 first). If we use $X_5^{(n)}$ instead of X_5 in this equation, we find

$$\begin{aligned} &X_5^{(n)}\big(X_3(x, v), V_3(x, v)\big) - X_5^{(n)}(x, v) \\ &\quad = R_n(x)v^{n+1} + \mathcal{O}\big(v^{n+2}\big) \end{aligned}$$

for some remainder function $R_n(x)$. Now using $X_5^{(n+1)}$ with a not yet determined coefficient $C_{n+1}(x)$, and remembering that

$$X_3(x, v) = x + \mathcal{O}(v), \qquad V_3(x, v) = r(x)v + \mathcal{O}\big(v^2\big),$$

gives

$$\begin{aligned} &X_5^{(n+1)}\big(X_3(x, v), V_3(x, v)\big) - X_5^{(n+1)}(x, v) \\ &\quad = \big[X_5^{(n)}\big(X_3(x, v), V_3(x, v)\big) - X_5^{(n)}(x, v)\big] \\ &\qquad + \big[C_{n+1}\big(X_3(x, v)\big)\big(V_3(x, v)\big)^{n+1} \\ &\qquad - C_{n+1}(x)v^{n+1}\big] \\ &\quad = \big[R_n(x)v^{n+1} + \mathcal{O}\big(v^{n+2}\big)\big] \\ &\qquad + \big[C_{n+1}(x)\big(r(x)v\big)^{n+1} + \mathcal{O}\big(v^{n+2}\big) \\ &\qquad - C_{n+1}(x)v^{n+1}\big] \\ &\quad = \big(R_n(x) - \big(1 - r(x)^{n+1}\big)C_{n+1}(x)\big)v^{n+1} \\ &\qquad + \mathcal{O}\big(v^{n+2}\big), \end{aligned} \tag{33}$$

which shows us that the undetermined coefficient $C_{n+1}(x)$ must be chosen as

$$C_{n+1}(x) = \frac{R_n(x)}{1 - r(x)^{n+1}}. \tag{34}$$

Thus, if we have computed a truncated approximation $x^{*(n)} = X_5^{(n)}(x, v(x))$ of the point where chattering completes, we can both get an improved approximation of this point and an estimate of the truncation

error, by first taking another impact/flight, and then approximating the chattering point again, that is

$$\tilde{x}^{*(n)} = X_5^{(n)}\big(X_3\big(x, v(x)\big), V_3\big(x, v(x)\big)\big).$$

The improved chattering point is then

$$\frac{\tilde{x}^{*(n)} - r(x)^{n+1} x^{*(n)}}{1 - r(x)^{n+1}}$$

which is correct to order $v(x)^{n+1}$, and the error estimate is

$$X_5(x, v(x)) - X_5^{(n)}\big(x, v(x)\big) = \frac{\tilde{x}^{*(n)} - x^{*(n)}}{1 - r(x)^{n+1}} + \mathcal{O}\big(v(x)^{n+2}\big). \tag{35}$$

Note that we are assuming here that the impact/flight mappings X_3 and V_3 are known exactly. In practice they are computed through numerical integration, and we cannot trust the above estimate of the truncation error in X_5, unless the truncation errors in the numerical integration are known to be of smaller size.

3.5 Example: the bouncing ball

Consider the simplest possible example: a ball moving vertically under gravity and bouncing with a Newton coefficient of restitution e, where $0 \le e < 1$ (see Fig. 1). For this example all functions defined above can be explicitly computed, so this gives an illustration to how the theory works. We have

$$\ddot{q} = -g < 0, \quad q \ge 0, \qquad \dot{q}^+ = -e\dot{q}^-$$

when impacting at $q = 0$.

Letting $x = (x_1, x_2, x_3)^{\mathrm{T}}$, where $x_1 = q$, $x_2 = \dot{q}$ and x_3 is a variable to keep track of time, and rewriting the impact law in the form of Eqs. (2) and (5), we have

$$F(x) = \begin{pmatrix} x_2 \\ -g \\ 1 \end{pmatrix}, \qquad H(x) = x_1, \qquad v(x) = x_2,$$

$$W(x) = \begin{pmatrix} 0 \\ -(1+e) \\ 0 \end{pmatrix}.$$

From this we compute using (3), (8), (10) and (12) that

$$a(x) = -g, \qquad r(x) = e, \qquad \lambda(x) = -g/(1+e),$$

$$F'(x) = \begin{pmatrix} x_2 \\ 0 \\ 1 \end{pmatrix}.$$

The relevant Σ sets are

$$\Sigma_0^+ = \{x \mid x_1 > 0\}, \qquad \Sigma_1^- = \{x \mid x_1 = 0,\ x_2 < 0\},$$
$$\Sigma_1^+ = \{x \mid x_1 = 0,\ x_2 > 0\},$$
$$\Sigma_2^- = \{x \mid x_1 = 0,\ x_2 = 0\}.$$

We can now compute the end result according to (30) to be

$$x^* = x + \begin{pmatrix} -\frac{2ex_2}{g(1-e)} \\ -1 \\ -\frac{2e}{g(1-e)} \end{pmatrix} x_2 + x_2^2 \mathcal{O}(1). \tag{36}$$

If we only keep the two first terms, we find that the final velocity happens to be exactly 0, the time taken for chattering is also exact, but starting with $x_1 = 0$ we find that the final position is of the order x_2^2. This is of course consistent with the neglected term.

For this simple example, all equations defining the functions are actually solvable in closed form. Using (13) and (14) we find for the impact that

$$X_1(x, v) = x + \begin{pmatrix} 0 \\ -(1+e) \\ 0 \end{pmatrix} v, \qquad V_1(x, v) = -ev,$$

and for the flow, using (1), (19), (20) and (21), that

$$\phi(x, t) = \begin{pmatrix} x_1 + x_2 t - gt^2/2 \\ x_2 - gt \\ x_3 + t \end{pmatrix}, \qquad T_2(x, v) = \frac{2}{g} v$$

so

$$X_2(x, v) = x + \begin{pmatrix} \frac{2x_2}{g} \\ -2 \\ \frac{2}{g} \end{pmatrix} v + \begin{pmatrix} -\frac{2}{g} \\ 0 \\ 0 \end{pmatrix} v^2,$$

$$V_2(x, v) = -v.$$

For the next time mapping (22), (23) we get

$$X_3(x, v) = x + \begin{pmatrix} -\frac{2ex_2}{g} \\ -(1-e) \\ -\frac{2e}{g} \end{pmatrix} v + \begin{pmatrix} \frac{2e}{g} \\ 0 \\ 0 \end{pmatrix} v^2,$$

$$V_3(x, v) = ev.$$

Solving the stable manifold equation (28), inverting the result by solving (29), and inserting the expression for $v(x)$ finally gives

$$X_4(x,v) = x + \begin{pmatrix} \frac{2ex_2}{g(1-e)} \\ 1 \\ \frac{2e}{g(1-e)} \end{pmatrix} v,$$

$$X_5(x,v) = x + \begin{pmatrix} -\frac{2ex_2}{g(1-e)} \\ -1 \\ -\frac{2e}{g(1-e)} \end{pmatrix} v + \begin{pmatrix} \frac{2e}{g(1-e)} \\ 0 \\ 0 \end{pmatrix} v^2, \quad (37)$$

$$X_5(x,v(x)) = \begin{pmatrix} x_1 \\ 0 \\ x_3 + \frac{2e(-x_2)}{g(1-e)} \end{pmatrix}.$$

The formula (37) tells us that if we start in Σ_0^- with $x_1 = 0$, $x_2 = -v_0$, chattering completes in $2ev_0/(g(1-e))$ time units at $x_1 = 0$, $x_2 = 0$, which indeed belongs to Σ_1. Note also the error in position introduced by keeping only terms linear in v in (36) is gone in (37).

4 Stability analysis and continuation

4.1 Solution structure

Now that we have introduced the chatter mapping, as a way to bypass the accumulation of events associated with complete chattering, we can view the solution over a finite time interval as a finite sequence of trajectories of either F or F', connected by (possible non-instantaneous) events. This can be represented as follows.

The continuous trajectories are given by a sequence of functions $X_k : I_k \to \mathbb{R}^n$ ($k \in \{0, 1, \ldots, N\}$) where $I_k = [t_k, t_k']$ is a sequence of time intervals. Also we have a sequence of discrete states $S_k \in \{f, s\}$ (f for free flight, s for sticking) and vector fields $F_k : \mathbb{R}^n \to \mathbb{R}^n$, where

$$F_k = \begin{cases} F & \text{if } S_k = f \\ F' & \text{if } S_k = s. \end{cases}$$

Thus X_k is a trajectory of F_k in the time interval I_k, and for $t_k < t < t_k'$ we have $X_k(t) \in \Sigma_0^+$ if $S_k = f$, or $X_k(t) \in \Sigma_2^-$ if $S_k = s$.

Denoting the initial and final points of each trajectory by

$$x_k = X_k(t_k) \quad \text{and} \quad x_k' = X_k(t_k'),$$

respectively, we also have *event mappings* $E_k : \mathbb{R}^n \to \mathbb{R}^n$, $e_k : \mathbb{R}^n \to \mathbb{R}$, such that

$$x_{k+1} = E_k(x_k'), \quad (38)$$

$$t_{k+1} = t_k' + e_k(x_k'). \quad (39)$$

All this takes place at an *event surface* defined as the zero level set of a scalar function $H_k : \mathbb{R}^n \to \mathbb{R}$. From now on we will assume that all events are transversal, that is $\mathcal{L}_{F_k}(H_k)(x_k') \neq 0$, and that all flow time intervals have non-zero length. Then there are three possible events:

- If there is a complete chattering event, then $E_k = Q$, $e_k = q$, $H_k = H$, and we require $x_k' \in \Sigma_1^-$, $S_k = f$, $x_{k+1} \in \Sigma_2^-$, $S_{k+1} = s$.
- If there is a regular impact, then $E_k = R$, $e_k = 0$, $H_k = H$, and we require $x_k' \in \Sigma_1^-$, $S_k = f$, $x_{k+1} \in \Sigma_1^+$, $S_{k+1} = f$.
- Lastly, if we have a release from sticking, then $E_k = Id$ (the identity mapping), $e_k = 0$, $H_k = a$, and we require $x_k' \in \Sigma_3^+$, $S_k = s$, $S_{k+1} = f$.

Let us now impose the additional requirement that the initial and final points of the solution also stay clear of events, that is, both x_0 and x_N' belong to Σ_0^+ or Σ_2^-. Combined with the requirement of transversal events and non-zero time intervals, this means that all solutions starting at $\tilde{x}_0$ near x_0 will have the same number and type of events, albeit with slightly different time intervals in between. Solving for a given fixed time, so that $t_0 = \tilde{t}_0 = 0$, $t_N' = \tilde{t}_N' = T$, we can compute the final point corresponding to an initial point $\tilde{x}_0$ through the composition of mappings

$$\tilde{x}_N' = P(\tilde{x}_0) = (P_N \circ D_{N-1} \circ P_{N-1} \circ \cdots \circ D_0 \circ P_0)(\tilde{x}_0) \quad (40)$$

as long as $\tilde{x}_0$ is close to x_0. Here $P_k(x) = \phi_k(x, t_k' - t_k)$, where ϕ_k is the flow of vector field F_k (and where the times t_k' and t_k correspond to event times *for the point* x_0), and D_k is a *discontinuity mapping* corresponding to the event, which corrects for the fact that the event times of x_0 instead of $\tilde{x}_0$ have been used so the argument of D_k no longer lies exactly on the

event surface $H_k(x) = 0$. More precisely, the mapping $D_k(x)$ is defined for points x close to the event surface of event k as

$$D_k(x) = \phi_{k+1}\big(E_k\big(\phi_k\big(x, \tau(x)\big)\big)\big), \\ t_{k+1} - t'_k - e_k\big(\phi_k\big(x, \tau(x)\big)\big) - \tau(x)\big), \quad (41)$$

where t_{k+1} and t'_k are independent of x, and the time $\tau(x)$ is the time to reach the nearby impact surface, defined implicitly by

$$H_k\big(\phi_k\big(x, \tau(x)\big)\big) = 0. \quad (42)$$

We see that the discontinuity mapping always advances time by the fixed amount $d_k = t_{k+1} - t'_k$, it gives the same result as the event mapping for the point x'_k: $E_k(x'_k) = D_k(x'_k)$, $e_k(x'_k) = d_k$, and if preceded by the flow ϕ_k and followed by flow ϕ_{k+1}, the resulting composite dynamics will be the correct one.

4.2 Computation of derivatives

For stability analysis, we would like to compute the Jacobian P_x of P. From the composition (40) we find

$$P_x(x_0) = P_{Nx}(x_N) D_{N-1x}(x'_{N-1}) P_{N-1x}(x_{N-1}) \cdots \\ \cdot D_{0x}(x'_0) P_{0x}(x_0).$$

The flow Jacobians P_k can be computed using the variational equations consisting of the matrix ODE system

$$\frac{dJ}{dt}(t) = F_{kx}\big(\phi_k(x_k, t)\big) J(t), \qquad J(0) = I,$$
$$P_{kx}(x_k) = J(t'_k - t_k).$$

The Jacobian of the discontinuity mapping for a non-instantaneous event, sometimes referred to as the *saltation matrix* [21], has the formula

$$D_{kx}(x'_k) = A + \frac{B_2 - AB_1}{d} C \quad (43)$$

where

$$A = E_{kx}(x'_k) - B_2 e_{kx}(x'_k), \qquad B_2 = F_{k+1}(x_{k+1}),$$
$$B_1 = F_k(x'_k), \qquad d = \mathcal{L}_{F_k}(H_k)(x'_k),$$
$$C = H_{kx}(x'_k),$$

derived using the chain rule repeatedly on (38–39, 41–42). We see that the condition of transversal events means that $d \neq 0$, so the discontinuity mapping Jacobian is well defined.

Thus, by treating complete chattering as a single non-instantaneous event, we can compute the Jacobian around a given solution, as long as all events are transversal and all flow times non-zero. Should higher-order derivatives be needed, they too can be computed from the composition (40) by using higher-order variational equations and formulae for higher-order derivatives of the discontinuity mappings.

4.3 Scaling considerations

As we approach the tail of a complete chattering sequence, the impact velocity becomes smaller and smaller. Since the denominator in (43) is the impact velocity for events corresponding to regular impacts or complete chattering, the matrices D_k will have increasingly large elements as the events become less and less transversal. On the other hand, because we have shown that the event mapping for complete chattering is smooth, we know that these large elements must in fact cancel out. Numerically, however, we see that there is a risk of accuracy loss due to cancellation, if we wait too long before using the chattering map, especially if $H(x)$ is more complex than just the value of one of the coordinates. We can make the system better scaled if we, when a complete chattering sequence is suspected, introduce two new state variables: u which is the outgoing velocity of the latest impact, and h which is equal to $H(x)/u$. With the extended state variable

$$\hat{x} = \begin{pmatrix} x \\ h \\ u \end{pmatrix} \quad (44)$$

we use the extended impact mapping

$$\hat{x} \leftarrow \hat{R}(\hat{x}) = \begin{pmatrix} R(x) \\ 0 \\ v(R(x)) \end{pmatrix},$$

the extended impact surface function $\hat{H}(\hat{x}) = h$ and the extended vector field

$$\dot{\hat{x}} = \hat{F}(\hat{x}) = \begin{pmatrix} F(x) \\ v(x)/u \\ 0 \end{pmatrix}.$$

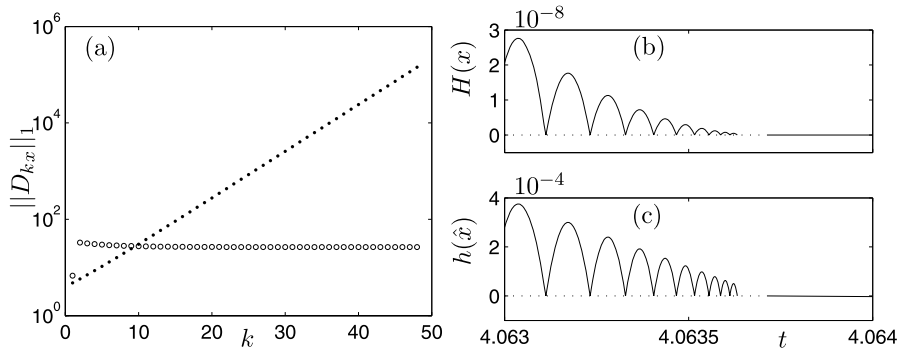

Fig. 3 (**a**) The norm $\|D_{kx}\|_1$ of the Jacobian of the discontinuity mapping at the kth impact in a chattering sequence (see (43)) when using the original (•) and extended (○) systems for an impacting ball. The value of $H(x)$ (**b**) and $h(\hat{x})$ (**c**) versus time in the tail of the complete chattering sequence of the bouncing ball in (a)

Then we find that the transversality quantity $\mathcal{L}_{\hat{F}}(\hat{H})(\hat{x})$ will instead converge to -1 as the impact velocity decreases, and the problem with small numbers in the denominator disappears (see Fig. 3(a), where $\|D_k\|_1$ versus k is plotted). Using $h = 0$ instead of $H(x) = 0$ also avoids problems with scaling in the event detection. In Figs. 3(b) and (c) we compare the values of H and h in the tail of a complete chattering sequence for an impacting ball (cf. Sect. 3.5 and Fig. 1). Notice especially the different scales on the vertical axes and the rate in which the envelopes decrease to zero. Note also the jumps in time that occur at the chattering events.

4.4 On the behavior of the Jacobian during a complete chattering sequence

Just after a complete chattering sequence, the system is in a sticking phase, and the Jacobian P_x must have at least co-rank 2 since $H_x P_x = 0$ and $v_x P_x = 0$. In fact, this loss of rank can be viewed as taking place in two distinct phases. By changing the final time T we can study the evolution of P_x, keeping in mind that P_x is double valued at times of impact, and is left undefined during the time jump associated with the complete chatter mapping. This later difficulty disappears if we postpone the use of the chatter mapping.

Suppose that the system completes chattering at state x^* and time t^*, with $a(x^*) < 0$, and that we are using the extended system introduced above in Sect. 4.3. The product of the impact and subsequent flow Jacobians is

$$\hat{P}_{k\hat{x}}(\hat{x}_k)\hat{D}_{k-1\hat{x}}(\hat{x}'_{k-1}) = A(x^*) + \mathcal{O}\big(v(x'_{k-1})\big)$$

where

$$A(x^*) = \begin{pmatrix} I & 0 & 0 \\ 0 & 1 & 0 \\ 0 & 0 & 0 \end{pmatrix} + \begin{pmatrix} W(x^*) \\ 2r(x^*)/a(x^*) \\ -r(x^*) \end{pmatrix} \begin{pmatrix} v_x(x^*) & a(x^*) & 0 \end{pmatrix}.$$

Here the second-to-last row and column correspond to the extended variable h, and the last row and column to u. $A(x^*)$ has n eigenvalues equal to 1 and two eigenvalues equal to r and 0 respectively. The subspace invariant under $A(x^*)$ is spanned by

$$\begin{pmatrix} I \\ -v_x(x^*)/a(x^*) \\ 0 \end{pmatrix}.$$

If we write

$$p_k = \hat{P}_{k\hat{x}}(\hat{x}_k)\hat{D}_{k-1\hat{x}}(\hat{x}'_{k-1})\hat{P}_{k-1\hat{x}}(\hat{x}_{k-1})\cdots \cdot D_{0x}(x'_0)P_{0x}(x_0)$$

(the switch to extended variables occurs somewhere before event $k-1$), then

$$p_{k+1} = \big(A(x^*) + \mathcal{O}\big(v(x'_k)\big)\big)p_k$$

and since $v(x'_k) \to 0$ like r^k, the matrices p_k will converge to a matrix p_∞ that is invariant under $A(x^*)$. Now we are mostly interested in the upper n rows of p_k (corresponding to the original variables), so let us call that submatrix

$$J_k = \begin{pmatrix} I & 0 & 0 \end{pmatrix} p_k.$$

The h and u dependence on the initial condition, as recorded by the two last rows of p_k, is bounded,

and we also know that the values of both h and u decrease like $r(x^*)^k$. Thus the dependence of $H = hu$ on initial conditions must also be $\sim r(x^*)^k$. Therefore we conclude that $H_x(x^*)J_\infty = 0$. We have no reason to expect any other loss of rank, and thus towards the end of the chattering sequence,

$$J_k = J_\infty + \mathcal{O}\big(v(x'_{k-1})\big),$$

and J_∞ in general has co-rank 1.

Finally, if we put the chattering map back again, the Jacobian of the discontinuity mapping associated with complete chattering (and also dropping the extended variables) is $\hat{D}_{K\hat{x}}(\hat{x}'_K) = D(x^*) + \mathcal{O}(v(x'_K))$, where

$$D(x^*) = \begin{pmatrix} I - \dfrac{W(x^*)v_x(x^*)}{v_x(x^*)W(x^*)} & 0 & 0 \end{pmatrix}, \tag{45}$$

and clearly $v_x(x^*)D(x^*) = 0$.

In the original variables, the behavior of the Jacobian P_x during a chattering sequence is that $H_x P_x \to 0$ like r^k, where k is the number of impacts during the chattering sequence, while $v_x P_x$ converges to a nonzero value. At the moment the sequence completes, $v_x P_x$ also jumps to 0.

We finish by illustrating the behavior of the Jacobian for the bouncing ball problem (see Sect. 3.5). Assume that the ball is released from rest at the height $s > 0$:

$$x_0 = \begin{pmatrix} s \\ 0 \end{pmatrix}. \tag{46}$$

Reconstructing the extended state variables h and u from the initial conditions, we find the Jacobian $\hat{P}_{0x}$ of the extended state with respect to the two components of the initial conditions after the first flight, the Jacobian $\hat{D}_{k\hat{x}}$ of any subsequent impact discontinuity mapping, and the Jacobian $\hat{P}_{k\hat{x}}$ of any subsequent flight:

$$\hat{P}_{0x} = \begin{pmatrix} 1 & -\frac{v'_0}{g} \\ 0 & 1 \\ -\frac{1}{v'_0} & \frac{1}{g} \\ -\frac{g}{v'_0} & 0 \end{pmatrix},$$

$$\hat{D}_{k\hat{x}} = \begin{pmatrix} 1 & 0 & (1+e)v'_k & 0 \\ 0 & -e & (1+e)g & 0 \\ 0 & 0 & -1 & 0 \\ 0 & -e & eg & 0 \end{pmatrix}, \tag{47}$$

$$\hat{P}_{k\hat{x}} = \begin{pmatrix} 1 & \frac{2v_k}{g} & 0 & 0 \\ 0 & 1 & 0 & 0 \\ 0 & \frac{2}{g} & 1 & 0 \\ 0 & 0 & 0 & 1 \end{pmatrix},$$

where the first impact velocity is $v'_0 = -\sqrt{2gs}$, and $v'_k = -v_k = e^k v'_0$. Recall that $0 \le e < 1$. We compute

$$\begin{aligned} p_n &= \left(\prod_{k=1}^{n} \hat{P}_{k\hat{x}} \hat{D}_{k-1\hat{x}}\right) \hat{P}_{0x} \\ &= \frac{1}{1-e} \begin{pmatrix} e^n(1+e-2e^{n+1}) & -\frac{v'_0}{g}e^n(1-e) \\ -\frac{g}{v'_0}(1+e)(1-e^n) & 1-e \\ -\frac{1}{v'_0}(1+e-2e^{n+1}) & \frac{1}{g}(1-e) \\ -\frac{g}{v'_0}e^n(1-e^n) & 0 \end{pmatrix}, \end{aligned} \tag{48}$$

which indeed is $\mathcal{O}(v'_n) = \mathcal{O}(e^n)$ close to the limit matrix p_∞. The dependence of the original two state variables, that is given by the matrices J_k consisting of the two top rows of each p_k, shows that the H dependence (the first row) converges to 0 like e^n, whereas the second row (the v dependence) converges to nonzero values.

We can replace the tail of the chattering sequence by applying the chattering map (and dropping extended variables) after flight with N impacts. Since we have an exact expression for this event mapping (see (37))

$$\hat{E}_N(\hat{x}) = \begin{pmatrix} x_1 \\ 0 \end{pmatrix}, \qquad \hat{e}_N(\hat{x}) = \frac{-2ex_2}{g(1-e)}, \tag{49}$$

we can compute the Jacobian $\hat{D}_{N\hat{x}}$ of the corresponding discontinuity mapping and finally the Jacobian $\hat{D}_{N\hat{x}p_N}$ of the state after chattering completes with respect to the initial conditions:

$$\hat{D}_{N\hat{x}} = \begin{pmatrix} 1 & 0 & e^n v'_0 & 0 \\ 0 & 0 & 0 & 0 \end{pmatrix}, \qquad \hat{D}_{N\hat{x}p_N} = \begin{pmatrix} 0 & 0 \\ 0 & 0 \end{pmatrix}. \tag{50}$$

The last result shows that the sticking state is indeed independent of initial conditions. The time evolution of the derivative of the position and velocity with respect to the initial position are shown in Fig 4. We note the gradual decay to 0 for the position, and the sudden jump to 0 when chattering ends for the velocity.

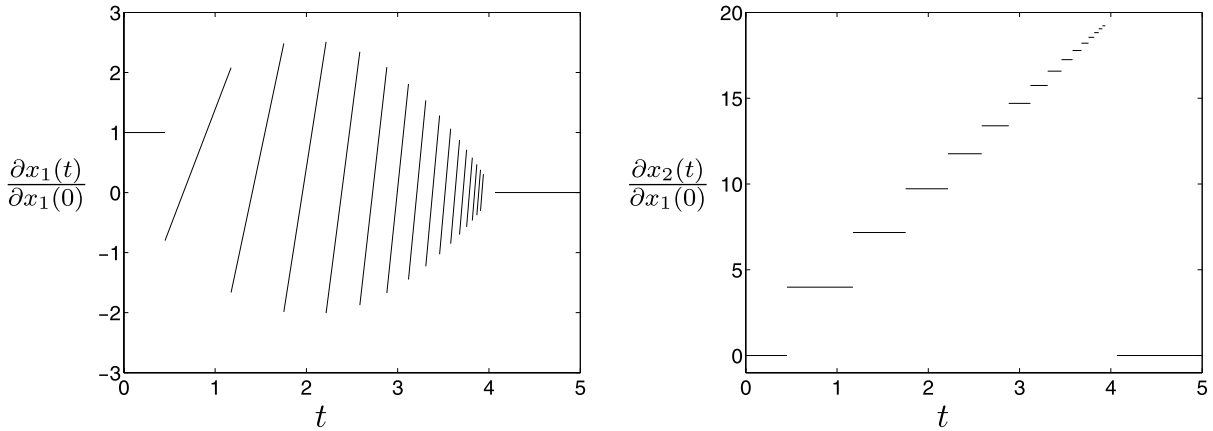

Fig. 4 Time evolution of two components of the Jacobian matrix for the bouncing ball with $g = 9.8$ and initial height $s = 1$. *Left*: $\frac{\partial x_1(t)}{\partial x_1(0)}$, *right*: $\frac{\partial x_2(t)}{\partial x_1(0)}$. The chattering map was applied at $N = 15$

5 Numerical scheme

In this section we will describe our proposed numerical scheme for solving impacting systems with one impacting surface. In particular we will focus on transitions that occur at various events, such as at impacts and release from stick.

To solve impacting systems with a hybrid-system approach (see Sect. 1) is basically the same as solving any smooth system since in both cases a smooth solver is used to solve IVPs. The main difference is that when an event is detected in an impact problem, a discontinuity map is applied and a new IVP is solved.

As with any ODE solver for smooth systems, one first has to give a vector field, initial conditions, simulation times and various tolerances. On top of this, information about the impact surface and the impact law at the surface has to be provided.

In what follows we will assume that an ODE solver for smooth systems combined with an event-detection routine exists. Therefore the focus will be on the local maps, state shifts and the logic used to keep track on what system of ODEs to use in a particular situation. Also, to show that our proposed methodology works for both simulation and stability analysis we have in Sect. 6 used a simulation driver that is based on the methodology described here on top of one of MATLAB's ODE solvers that has a built-in event-detection routine. However, it is of course possible to write your own ODE solver and event-detection routine, which could for instance be based on interval halving or the secant method.

Let us now describe what the proposed simulation driver for impacting systems with chattering can look like.

5.1 Simulation driver

The basic idea for the simulation driver using the hybrid-system approach is based on discrete states S_k. Following the methodology described in Sect. 4.1, there are two discrete states, $S_k = f$ for the free flight and $S_k = s$ for sticking, and three possible events that can occur. When solving an IVP with a time stepper it is well known that near-grazing zero crossings are often missed. Therefore we will extend this idea in two steps.

Let us first make the basic idea described above more robust from a numerical point of view by extending S_k so that

$$S_k = \begin{cases} f^+, & x \in S_1^+, \\ f^-, & x \in S_1^-, \\ s, & x \in \Sigma_2^- \end{cases} \quad \text{and}$$
$$F_k = \begin{cases} F, & S_k \in \{f^+, f^-\}, \\ F', & S_k = s. \end{cases} \tag{51}$$

Five different events can now occur: (i)—an impact with negative velocity, (ii)—a complete chattering event, (iii)—release from stick, (iv)—negative velocity becomes positive, and (v)—positive velocity becomes negative. A flow diagram of this is presented in Fig. 5(a).

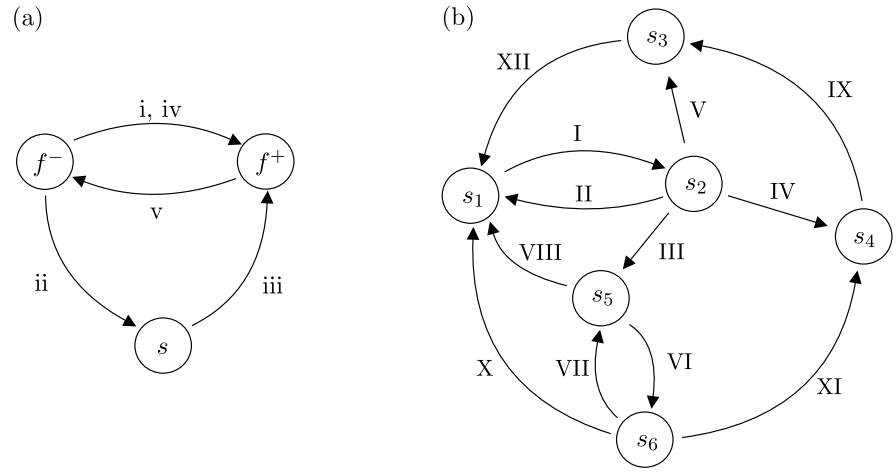

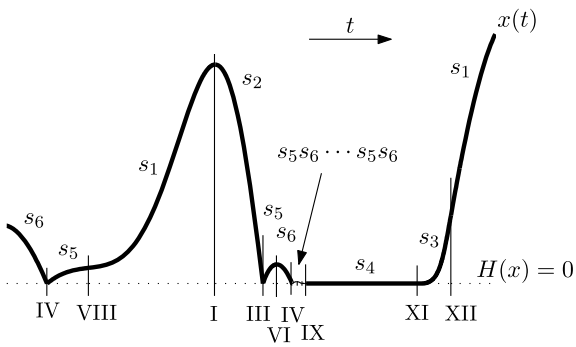

Fig. 6 A schematic description of the time history for a state variable $x(t)$ from an impacting system. The impacting surface is given by the scalar function $H(x) = 0$ and the different states, used in the simulation algorithm, are given by $s_i, i = 1, \ldots, 6$. The *roman numerals* correspond to some of the transitions described in the flow diagram in Fig. 5

Secondly, if we use the same idea as in Fig. 5(a) but also introduce the extended state and vector field introduced in Sect. 4.3, we end up with a slightly more complicated situation. To deal with this, we define six states, s_i for $i = 1, \ldots, 6$, to keep track on what ODEs to use, what events to look for, and what state variables to use, the original or the extended (see (44)). In Fig. 6 we present a schematic trajectory corresponding to a general dynamical system

$$\dot{x} = f(x, t), \quad x \in \mathbb{R}^n$$

with an impacting surface at $H(x) = 0$. In the figure we have indicated where the different events occur with Roman numerals (see further, Fig. 5(b)). In between the events the system is in one of the different states s_i and transitions from one state to another occur at the events. Short descriptions of the different states are given below:

State s_1: Free flight with $v(x) > 0$. Impacts are not possible.

State s_2: Free flight with $v(x) < 0$. Impacts are possible.

State s_3: Free flight with $v(x) > 0$, $a(x) > 0$. Impacts are not possible.

State s_4: Stick phase with $v(x) = 0$, $a(x) < 0$.

State s_5: Free flight with $\hat{v}(\hat{x}) > 0$, $\hat{a}(\hat{x}) < 0$. Impacts are not possible.

State s_6: Free flight with $\hat{v}(\hat{x}) < 0$. Impacts are possible.

Recall that $v(x)$ and $a(x)$ are respectively the velocity and acceleration relative to the impacting surface (cf. (2) and (3)). Notice also that $\hat{x}$, $\hat{v}(\hat{x})$ and $\hat{a}(\hat{x})$ are the extended state, the extended relative velocity and acceleration, respectively. The states s_1–s_4 use the original state variable x and in states s_5 and s_6 the extended state variable $\hat{x}$ is used with a different event function to locate the impacting surface (see Sect. 4.3).

To further clarify how our proposed algorithm works, we show in Fig. 5(b) a flow diagram over the transitions between the states s_1–s_6. The Roman numerals I–XII correspond to the event locations (zero crossings), state transitions, and discontinuity mappings at specific events (cf. Fig. 6). In Table 1 we have listed, from left to right, the transition labels, zero-crossing functions, accelerations at the events, state transitions and local mappings. In the second column we have listed what zero crossing to looking for to

Table 1 A table corresponding to the time history in Fig. 6 and the flow diagram in Fig. 5 that shows the transition label, what zero crossing to look for to get a specific event, and the acceleration, state transition and the local mapping at that event

Transition	Zero crossing	Acceleration	State	Mapping
I	$v(x)\downarrow 0$	$a(x)\lessgtr 0$	$s_1 \to s_2$	$x \to x$
II	$v(x)\uparrow 0$	$a(x) > 0$	$s_2 \to s_1$	$x \to x$
III	$H(x)\downarrow 0$	$a(x) < 0$	$s_2 \to s_5$	$x \to \hat{x} \to \hat{R}(\hat{x})$
IV	$H(x)\downarrow 0$	$a(x) < 0$	$s_2 \to s_4$	$x \overset{r=0}{\to} R(x)$
V	$H(x)\downarrow 0$	$a(x) > 0$	$s_2 \to s_3$	$x \overset{r=0}{\to} R(x)$
VI	$\hat{v}(\hat{x})\downarrow 0$	$\hat{a}(\hat{x}) < 0$	$s_5 \to s_6$	$\hat{x} \to \hat{x}$
VII	$h(\hat{x})\downarrow 0$	$\hat{a}(\hat{x}) < 0$	$s_6 \to s_5$	$\hat{x} \to \hat{R}(\hat{x})$
VIII	$\hat{a}(\hat{x})\uparrow 0$	$a(x) = 0$	$s_5 \to s_1$	$\hat{x} \to x$
IX	$\hat{v}(\hat{x})\downarrow 0$	$\hat{a}(\hat{x}) < 0$	$s_6 \to s_4$	$\hat{x} \to \hat{Q}(\hat{x}) \to x, t \to \hat{q}(\hat{x})$
X	$\hat{v}(\hat{x})\uparrow 0$	$\hat{a}(\hat{x}) > 0$	$s_6 \to s_1$	$\hat{x} \to x$
XI	$a(x)\uparrow 0$	$a(x) = 0$	$s_4 \to s_3$	$x \to x$
XII	$a(x)\downarrow 0$	$a(x) = 0$	$s_3 \to s_1$	$x \to x$

get the transition in the corresponding row, and also if the zero crossing is from negative to positive ($\uparrow$) or positive to negative ($\downarrow$).

5.2 Error checking for the complete chattering event

At the complete chattering event there are two things that the algorithm has to check for. First, the algorithm has to make sure that the acceleration after the complete chattering mapping is negative, i.e. $a(E_k(x_k')) < 0$ (see (38)), so that there will indeed be a transition to sticking. Second, to make sure that the error of using the approximate mapping at the complete chattering event is within the numerical tolerance, the method calculates x_{k+1}, t_{k+1}, given by (30) and (31), using the acceleration both at x_k', t_k' and at x_{k+1}, t_{k+1}. When the difference between these mappings is of the order of the tolerance, the method goes ahead with the complete chattering mapping. However, this method can be improved by comparing two consecutive impacts along the lines discussed in Sect. 3.4. An analysis of the proposed and an improved error indicator is given next.

5.2.1 Analysis of the error indicator

Recall the analysis in Sects. 3.1–3.4 and assume that

$$X_3(x, v) = x + K(x)v + A(x)v^2 + \mathcal{O}\big(v^3\big),$$
$$V_3(x, v) = r(x)v + B(x)v^2 + \mathcal{O}\big(v^3\big),$$

for some coefficients $A(x)$ and $B(x)$, and that the first-order truncation of X_5 is $X_5^{(1)}(x, v) = x + C_1(x)v$. From this we can compute the error estimate (cf. (35))

$$\begin{aligned} &X_5(x, v) - X_5^{(1)}(x, v) \\ &\quad = \frac{A(x) + C_1(x)B(x) + r(x)C_{1x}(x)K(x)}{1 - r(x)^2}v^2 \\ &\qquad + \mathcal{O}\big(v^3\big). \end{aligned}$$

Above, in Sect. 5.2, it is mentioned that the error indicator

$$\begin{aligned} &X_5(x, v) - X_5^{(1)}(x, v) \\ &\quad \sim x + C_1\big(X_5^{(1)}(x, v)\big)v - X_5^{(1)}(x, v) \\ &\quad = \frac{C_{1x}(x)K(x)}{1 - r(x)}v^2 + \mathcal{O}\big(v^3\big) \end{aligned}$$

is instead used. We see that this indicator neglects the influence of the v^2 terms in X_3 and V_3, and that it is further off by a factor $r(x)/(1 + r(x))$. This suggests that if it is possible to simulate an extra impact, before using the map at the chattering event, this should be done in order to find a better error estimate.

6 Example

Consider a double pendulum subject to gravitational acceleration g, depicted in Fig. 7, where q_1 is the absolute angle of the upper bar with length L_1 and q_2 is the absolute angle of the lower bar with length L_2. The two bars are considered to be massless, but the end-point of each bar has mass m_1 and m_2, respectively. Both joints are rigid and at the upper joint a

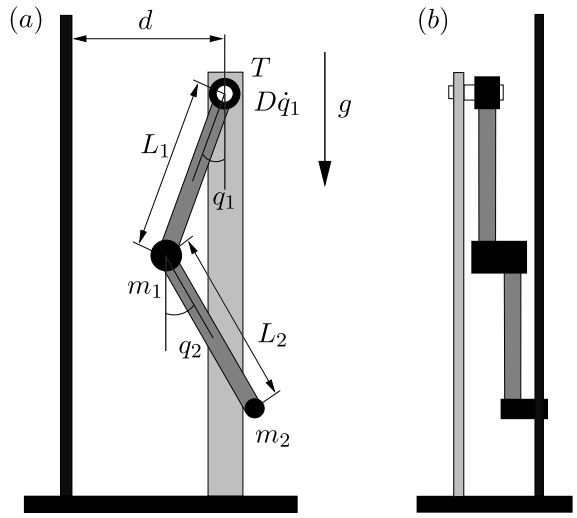

Fig. 7 The (**a**) front and (**b**) side view of a forced double pendulum with a unilateral constraint

constant torque T and viscous damping $D\dot{q}$ are applied, where D is the damping coefficient, while the lower joint is considered frictionless. The lower mass can impact with a rigid wall, a horizontal distance d away from the upper joint. A restitution law is applied when impacting.

By letting

$$q = (q_1 \quad q_2)^{\mathrm{T}}, \qquad \dot{q} = (\dot{q}_1 \quad \dot{q}_2)^{\mathrm{T}}$$

and

$$s_i = \sin(q_i), \qquad c_i = \cos(q_i), \qquad s_{ij} = \sin(q_i - q_j),$$
$$c_{ij} = \cos(q_i - q_j),$$

the horizontal and vertical positions of the impacting mass m_2 relative to the upper joint can be written

$$X(q) = L_1 s_1 + L_2 s_2 \quad \text{and} \quad Y(q) = -(L_1 c_1 + L_2 c_2),$$

respectively. Consequently, the distance from the lower mass m_2 to the rigid wall can be written as

$$H(q) = X(q) + d, \tag{52}$$

and thus an impact occurs as $H(q) = 0$. The equations of motion for this system can be written as

$$M(q)\ddot{q} + L(q,\dot{q}) + V(q) = K(q)\dot{q} + \lambda N(q), \tag{53}$$

where

$$M(q) = \begin{pmatrix} (m_1+m_2)L_1^2 & m_2 L_1 L_2 c_{12} \\ m_2 L_1 L_2 c_{12} & m_2 L_2^2 \end{pmatrix},$$

$$L(q,\dot{q}) = L_1 L_2 s_{12} \begin{pmatrix} m_1 \dot{q}_2^2 \\ m_2 \dot{q}_1^2 \end{pmatrix},$$

$$V(q) = \begin{pmatrix} (m_1+m_2) g L_1 s_1 - T \\ m_2 g L_2 s_2 \end{pmatrix},$$

$$K(q) = \begin{pmatrix} -D & 0 \\ 0 & 0 \end{pmatrix},$$

$$N(q) = \left(\frac{dH(q)}{dq}\right)^{\mathrm{T}} = (L_1 c_1 \quad L_2 c_2)^{\mathrm{T}},$$

and where λ is a Lagrange multiplier.

If we let $\dot{q}^-$ and $\dot{q}^+$ be the velocity just before and just after impact, respectively, we have at impact that

$$M(\dot{q}^+ - \dot{q}^-) = -N\Lambda, \tag{54}$$
$$N^{\mathrm{T}}\dot{q}^+ = -eN^{\mathrm{T}}\dot{q}^-, \tag{55}$$

where $N\Lambda$ is the impulse and e is the restitution coefficient. Equations (54) and (55) can be written as

$$\begin{pmatrix} M & N \\ N^{\mathrm{T}} & 0 \end{pmatrix} \begin{pmatrix} \dot{q}^+ \\ \Lambda \end{pmatrix} = \begin{pmatrix} M\dot{q}^- \\ -eN^{\mathrm{T}}\dot{q}^- \end{pmatrix}, \tag{56}$$

and solving (56) yields

$$\Lambda = \frac{(1+e)}{N^{\mathrm{T}}M^{-1}N} N^{\mathrm{T}}\dot{q}^-, \tag{57}$$

$$\dot{q}^+ = \dot{q}^- - \frac{M^{-1}N(1+e)}{N^{\mathrm{T}}M^{-1}N} N^{\mathrm{T}}\dot{q}^-, \tag{58}$$

and if we use $x = (q^{\mathrm{T}} \ \dot{q}^{\mathrm{T}})^{\mathrm{T}}$ as our state variable, we get the vector field F as

$$F = \begin{pmatrix} \dot{q} \\ M^{-1}(q)(-L(q,\dot{q}) - V(q) + K(q)\dot{q}) \end{pmatrix} \tag{59}$$

and the impact law can be written as (5), where

$$W = \begin{pmatrix} 0 \\ -\frac{M^{-1}N(1+e)}{N^{\mathrm{T}}M^{-1}N} \end{pmatrix}.$$

Now we have all information we need to simulate trajectories that have both impacts and chattering sequences, as well as calculate the stability of periodic orbits and continue them under parameter variations.

In what follows we will look at three typical scenarios, namely, transition from periodic orbits with complete chattering to motion with incomplete chattering, and local (period-doubling) and global (homoclinic) bifurcations. In the three examples we let

$$g = 9.81, \quad m_1 = 1, \quad m_2 = 2, \quad L_1 = L_2 = 1,$$
$$D = 10$$

and we will vary e, T an d in order to highlight the different aspects of impacting systems with chattering mentioned above. Also we demonstrate that our proposed simulation algorithm works in the way one would expect.

6.1 Transition from complete to incomplete chattering

Consider the double pendulum with vector field (59) and let $d = 0.5$ and $T = -31.15$. First we let the coefficient of restitution be $e = 0.89$. For this value of e we have a stable period-1 orbit with complete chattering, as shown in Fig. 8(a). In the figure we have indicated the non-zero time spent in sticking mode as $\tau > 0$. To see what happens to the stable period-1 orbit as e is increased we calculated a brute-force bifurcation diagram, which can be seen in Fig. 8(b). It is clear that there is a transition from a stable period-1 orbit to some other attractor. What happens here is that as e is increased the time τ spent in sticking mode is decreased until ultimately τ becomes 0 for some e^*. Precisely what happens to the orbit at e^* is that there is an infinite number of impacts that end at a point in Σ_3^+, so that no sticking can occur. In Fig. 8(c) a part of a trajectory for $e = 0.896$ is depicted to show the special situation where there is a finite, but large, number of impacts.

The continuous transformation of a trajectory like (a) into one like (c) clearly involves the loss of an infinite number of impacts, and at a point where the number of impacts decreases, the trajectory must have a grazing impact. Thus we expect that the parameter value e^* is the accumulation point of an infinite sequence of grazing bifurcation points. Preliminary theoretical analysis on one-degree of freedom models [26] leads us to conjecture that the size of the attractor for $e > e^*$ is asymptotically proportional to $(e - e^*)^\kappa$, where κ is very close to but slightly larger that 1.2. This means that the size of the attractor is continuous at e^*, which is indicated in Fig. 8(b). Although the attractors in Fig. 8(b) seem to be mostly chaotic, we conjecture that asymptotically the attractor should be a stable finite number of impact period-1 orbits similar to Fig. 8(c) with a probability approaching 1, as $e \to e^*$.

6.2 Period-doubling bifurcation

Consider the double pendulum and let $e = 0.19$, $T = -40$. For $d = 0.5009$ a stable period-2 orbit with two time intervals of sticking can be located, which is depicted in Fig. 9(a). The Poincaré section is given by $q_1 - \pi/2 = 0$ so one period corresponds to one revolution of the upper bar. A brute-force bifurcation diagram, see Figs. 9(b) and (c), reveals that as the distance to the impacting surface is increased the period-2 orbit undergoes a period-doubling cascade, and the first period-doubling bifurcation occurs at $d \approx 0.5010$. To

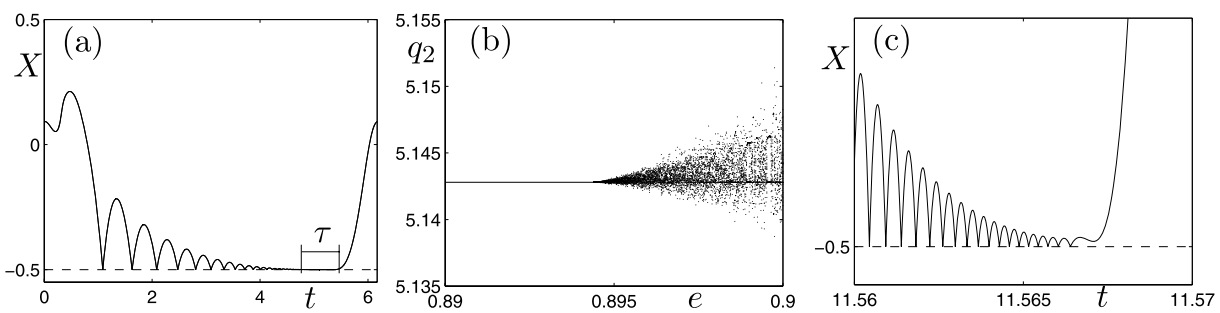

Fig. 8 (**a**) A time history of the lower mass X for one period of the system where $e = 0.89$. The trajectory has a complete chatter sequence and the time spent sliding is $\tau > 0$. (**b**) A brute-force bifurcation diagram showing q_2 versus the coefficient of restitution e at the Poincaré section $q_1 - \frac{\pi}{2} = 0$. (**c**) A time history of the lower mass X with an incomplete chattering sequence and where the time spent in sticking phase is $\tau = 0$ for $e = 0.896$. In all three figures $d = 0.5$ and $T = -31.15$

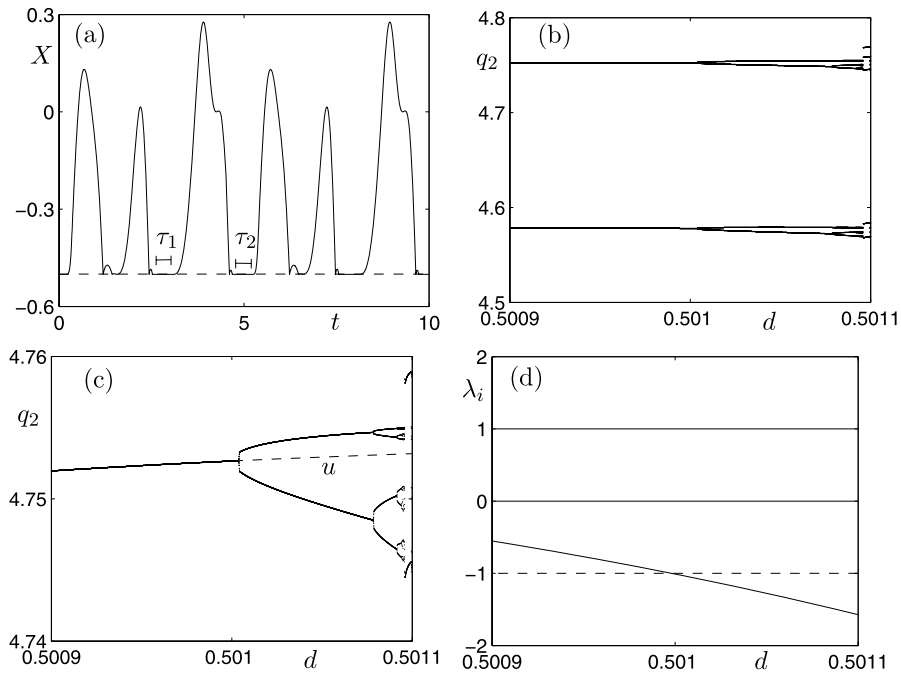

Fig. 9 (**a**) A trajectory for the lower mass m_2 for $d = 0.5009$, $e = 0.19$, $T = -40$. The scalars τ_1 and τ_2 represent two intervals of sticking motion. (**b**) A brute-force bifurcation diagram and (**c**) a zoom-in, where the Poincaré section is $q_1 = \pi/2$. (**d**) The eigenvalues λ_i corresponding to the branch of period-2 limit cycles in (b) and (c). The *dashed line* represents $\lambda_i = -1$

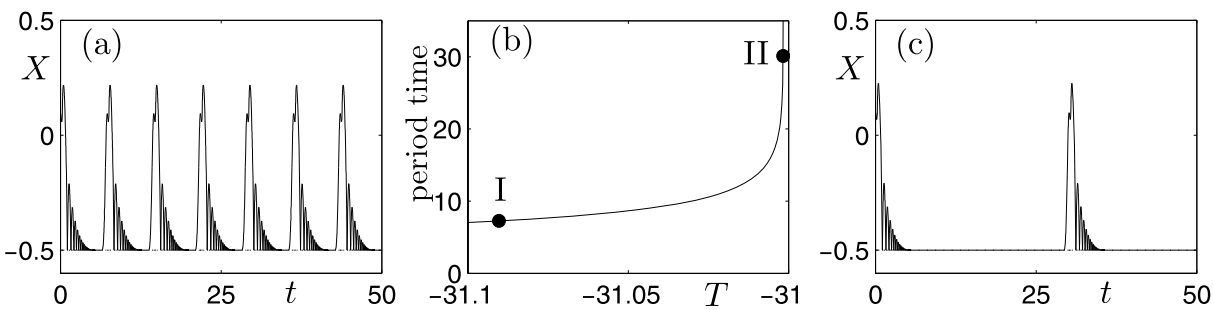

Fig. 10 (**a**) A time series for $X(t)$ showing seven periods of a stable period-1 orbit for $T \approx -31.09$, which corresponds to the point I in (b). (**b**) The period time versus the torque T when continuing a stable period-1 orbit. Trajectories corresponding to the points I and II can be seen in (a) and (b), respectively. (**c**) A time series for $X(t)$ showing about 1.7 periods of a stable period-1 orbit for $T \approx -31.0017$, which corresponds to the point II in (b)

verify that the proposed algorithm for stability analysis performs as it should, we continued the periodic orbit in Fig. 9(a) as the parameter d was varied. In Fig. 9(c) the unstable part of the branch is denoted with a 'u' and the corresponding eigenvalues are shown in Fig. 9(d). Recall that when an eigenvalue λ_i for a periodic orbit becomes -1 the system undergoes a period-doubling bifurcation, and one of the eigenvalues is 1 since the trajectory is a limit cycle.

6.3 Homoclinic bifurcation

Consider the double pendulum and let $d = -0.5$, $e = 0.9$. For $T \approx -31.09$ there exists a stable period-1 orbit, with a period time of $\approx$7.25, which is depicted in Fig. 10(a). By varying the torque T it is possible to continue this stable period-1 orbit and record the period time of the orbit. The change in period as the torque T varies is shown in Fig. 10(b). It is clear that as T approaches -31 the slope of the curve and the period increase. In Fig. 10(c) approximately 1.7 periods of the motion at the point II in Fig. 10(b) are shown. We can see that the free-flight motion and the complete chattering sequence are very similar in both the cases depicted in Figs. 10(a) and (c), but the main difference is the time spent sticking. This behavior suggests that there is a homoclinic orbit for a nearby parameter

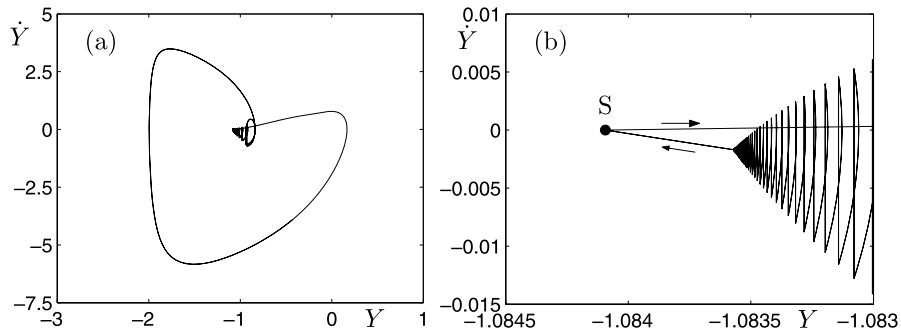

Fig. 11 (**a**) A projected phase portrait showing $\dot{Y}$ versus Y for $T \approx -31.001666$ with a period time of ≈ 76.26. (**b**) A zoom-in of the projected state portrait in (a), in a vicinity of the saddle equilibrium S. The *arrows* show the direction of the flow

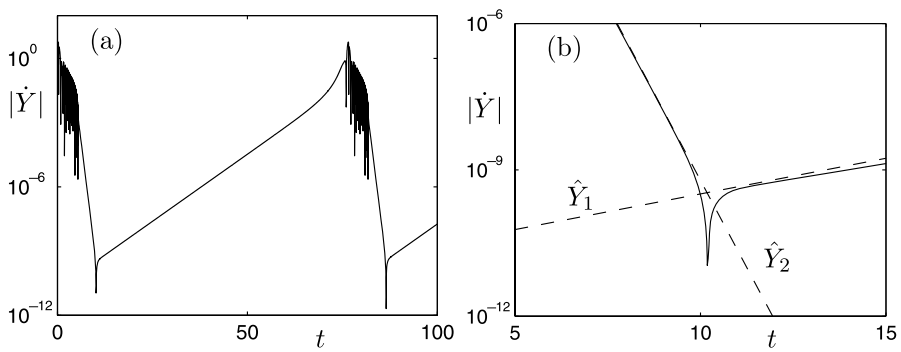

Fig. 12 (**a**) A time history of $|\dot{Y}|$ corresponding to the phase portrait in Fig. 11(a). (**b**) A close-up of (a) near the time when the trajectory of the periodic orbit passes that saddle equilibrium S in Fig. 11(b). Notice the logarithmic scale

value and thus there should exist a saddle equilibrium close to the periodic orbit. As it happens, this equilibrium is constrained to a surface where the lower mass is sticking against the impacting wall. Let us now take a closer look at this situation to verify that the proposed algorithms behave as they should in this situation.

Assuming that there is an equilibrium $(q, \dot{q}, \lambda) = (q^*, \dot{q}^* = 0, \lambda^*)$, we have from (53) that

$$V(q^*) = \lambda^* N(q^*), \tag{60}$$

$$H(q^*) = 0, \tag{61}$$

which can be solved numerically. For

$$T = -31.00166609425$$

the saddle equilibrium is given by

$$q_1^* = 4.91990567552337,$$

$$q_2^* = 0.49899755317827,$$

$$\lambda^* = 10.69293096743960,$$

with non-trivial eigenvalues

$$\mu_1 \approx 0.3366, \qquad \mu_2 \approx -3.2953.$$

For this specific value of T we show in Fig. 11(a) the projected phase plane Y–$\dot{Y}$ for the stable periodic orbit with period time ≈ 76.26. In Fig. 11(b) the close-up of Fig. 11(a) in a vicinity of the saddle equilibrium 'S' is shown. It is clear from Fig. 11(b) that the trajectory comes very close to the saddle equilibrium before it leaves the same.

In Fig. 12(a) the time series of $|\dot{Y}|$ corresponding to the projected phase diagram is shown and we see that the magnitude of the velocity $\dot{Y}$ is very small, as expected for a periodic orbit close to a homoclinic orbit. Let now

$$\hat{Y}_i(t) = e^{-21.8+\mu_i(t-\hat{t})}, \quad i = 1, 2,$$

where μ_i are the two eigenvalues for the saddle equilibrium and $\hat{t} = 10.17727070016352$. The two curves $\hat{Y}_i(t)$ are plotted in Fig. 12(b), and they confirm that the dynamics of the stable periodic orbit close to the saddle equilibrium is very similar to what one would have along its stable and unstable manifolds. This also confirms that our simulator gives the results as expected.

7 Discussion

In this manuscript we have introduced a novel numerical algorithm to simulate impacting systems with complete chattering. The new approach introduces a mapping that takes the state forward in time, bypassing the tail of complete chattering (that consists of an infinite number of impacts), and thus only a finite number of impacts needs to be handled in the simulation algorithm. We have chosen an event-driven approach since it is relatively straightforward to include the special mappings needed at the impacts and the tail of chattering sequences. Another important aspect of the proposed method is that it is possible to extend the pure simulator to also be able to perform stability analysis, by solving the first variational equations and merge the fundamental solution matrices from the free-flight phases with saltation matrices at the impacts and the complete chattering.

We showed that the method worked well for a forced double pendulum by numerically solving the equations of motion, locating periodic orbits, calculating their stability and continuing them under parameter variations. In particular we showed that the proposed methods can deal with situations that are common in impacting systems, namely, the loss of sticking and the location of local and global bifurcations.

The ultimate aim of this and similar work is to come up with numerical methods that can be included in numerical simulation packages, and make them available for not only specialists on non-smooth systems, but also to students, engineers and professionals simulating and analyzing some specific applications.

Acknowledgement This work was supported by the EU FP5 Project SICONOS (Grant No. IST-2001-37172).

References

1. Ascher, U.M., Petzold, L.R.: Computer Methods for Ordinary Differential Equations and Differential–Algebraic Equations. SIAM, Philadelphia (1998)
2. Beyn, W.-J., Champneys, A.R., Doedel, E., Govaerts, W., Kuznetsov, Yu.A., Sandstede, B.: Numerical continuation, and computation of normal forms. In: Handbook of Dynamical Systems, vol. 2, pp. 149–219. Elsevier Science, Amsterdam (2002). Chap. 4
3. Blakeborough, A.: An analytical approach of church bells to earthquake excitation. J. Earthq. Eng. **5**, 69–92 (2001)
4. Brogliato, B.: Impacts in Mechanical Systems—Analysis and Modelling. Lecture Notes in Physics, vol. 551. Springer, Berlin (2000)
5. Budd, C.J., Dux, F.: Chattering and related behaviour in impact oscillators. Phil. Trans. R. Soc. Lond. A **347**, 365–389 (1994)
6. Budd, C.J., Piiroinen, P.T.: Corner bifurcations in non-smoothly forced impact oscillators. Physica D **220**, 127–145 (2006)
7. Cunha, F.B., Pagano, D.J., Moreno, U.F.: Sliding bifurcations in planar variable structure systems. IEEE Trans. Circuit Syst. **50**(8), 1129–1134 (2003)
8. Dankowicz, H., Piiroinen, P.T.: Exploiting discontinuities for stabilization of recurrent motions. Dyn. Syst. **17**, 317–342 (2002)
9. Dercole, F., Kuznetsov, Yu.A.: SlideCont: An Auto97 driver for sliding bifurcation analysis. Department of Mathematics, Universiteit Utrecht, The Netherlands (2002)
10. di Bernardo, M., Budd, C.J., Champneys, A.R.: Grazing, skipping and sliding: analysis of the non-smooth dynamics of the DC/DC buck converter. Nonlinearity **11**, 858–890 (1998)
11. di Bernardo, M., Johansson, K.H., Vasca, F.: Self-oscillations and sliding in relay feedback systems: Symmetry and bifurcations. Int. J. Bifurc. Chaos **11**(4), 1121–1140 (2001)
12. di Bernardo, M., Kowalczyk, P., Nordmark, A.: Bifurcations of dynamical systems with sliding: derivation of normal-form mappings. Physica D **170**, 175–205 (2002)
13. di Bernardo, M., Budd, C.J., Champneys, A.R., Kowalczyk, P., Nordmark, A.B., Olivar, G., Piiroinen, P.T.: Bifurcations in non-smooth dynamical systems. SIAM Rev. **50**(4), 629–701 (2007)
14. di Bernardo, M., Budd, C.J., Champneys, A.R., Kowalczyk, P.: Piecewise Smooth Dynamical Systems—Theory and Applications. Springer, London (2008)
15. Doedel, E.J., Champneys, A.R., Fairgrieve, T.F., Kuznetsov, Yu.A., Sandstede, B., Wang, X.-J.: Auto97: Continuation and bifurcation software for ordinary differential equations (with HomCont). Computer Science, Concordia University, Montreal, Canada. ftp.cs.concordia.ca/doedel/doc/auto (1997)
16. Fredriksson, M.H., Borglund, D., Nordmark, A.B.: Experiments on the onset of impacting motion using a pipe conveying fluid. Nonlinear Dyn. **19**, 261–271 (1999)
17. Glocker, C.: Set-Valued Force Laws. Lecture Notes in Applied Mechanics, vol. 1. Springer, Berlin (2001)
18. Halse, C.K., Wilson, R.E., di Bernardo, M., Homer, M.E.: Coexisting solutions and bifurcations in mechanical oscillators with backlash. J. Sound Vib. **305**, 854–885 (2007)
19. Jerrelind, J., Stensson, A.: Braille printer dynamics. In: ASME Design Engineering Technical Conferences, DETC99/VIB-8032 (1999)
20. Kowalczyk, P., di Bernardo, M., Champneys, A.R., Hogan, S.J., Homer, M., Kuznetsov, Yu.A., Nordmark, A.B., Piiroinen, P.T.: Two-parameter non-smooth bifurcations of limit cycle: classification and open problems. Int. J. Bifurc. Chaos **16**(3), 601–629 (2006)
21. Leine, R.I., Nijmeijer, H.: Dynamics and Bifurcations of Non-Smooth Mechanical Systems. Lecture Notes in Applied and Computational Mechanics, vol. 18. Springer, Berlin (2004)
22. Nordmark, A.B.: Non-periodic motion caused by grazing incidence in impact oscillators. J. Sound Vib. **2**, 279–297 (1991)

23. Nordmark, A.B.: Universal limit mapping in grazing bifurcations. Phys. Rev. E **55**, 266–270 (1997)
24. Nordmark, A.B.: Existence of periodic orbits in grazing bifurcations of impacting mechanical oscillators. Nonlinearity **14**, 1517–1542 (2001)
25. Nordmark, A.B.: Discontinuity mappings for vector fields with higher-order continuity. Dyn. Syst. **17**, 359–376 (2002)
26. Nordmark, A.B.: On chattering bifurcations in 1 d.o.f. impact oscillator models. Manuscript in preparation
27. Nordmark, A.B., Kowalczyk, P.: A codimension-two scenario of sliding solutions in grazing-sliding bifurcations. Nonlinearity **19**, 1–26 (2006)
28. Osirio, G., di Bernardo, M., Santini, S.: Chattering and complex behavior of a can-follower system. In: ENOC-2005, Fifth Euromech Nonlinear Dynamics Conference (2005)
29. Peterka, F.: Part 1: Theoretical analysis of n-multiple $(1/n)$-impact solutions. CSAV Acta Tech. **19**, 462–473 (1974)
30. Peterka, F.: Results of analogue computer modelling of the motion. Part 2. CSAV Acta Tech. **19**, 569–580 (1974)
31. Pfeiffer, F., Glocker, Ch.: Multibody Dynamics with Unilateral Contacts. Wiley, New York (1996)
32. Piiroinen, P.T., Dankowicz, H.J.: Low-cost control of repetitive gait in passive bipedal walkers. Int. J. Bifurc. Chaos **15**(6), 1959–1973 (2005)
33. Shampine, L.F., Reichelt, M.W.: The MATLAB ODE suite. SIAM J. Sci. Comput. **18**, 1–22 (1997)
34. Shaw, S.W.: On the dynamic response of a system with dry friction. J. Sound Vib. **108**(2), 305–325 (1986)
35. Shaw, S.W., Holmes, P.J.: Periodically forced linear oscillator with impacts: chaos and long-periodic motions. Phys. Rev. Lett. **51**, 623–626 (1983)
36. Stronge, W.J.: Impact Mechanics. Cambridge University Press, Cambridge (2000)
37. Wagg, D.J., Karpodinis, G., Bishop, S.R.: An experimental study of the impulse response of a vibro-impacting cantilever beam. J. Sound Vib. **228**, 242–264 (1999)
38. Zhang, J., Johansson, K.H., Lygeros, J., Sastry, S.: Zeno hybrid system. Int. J. Robust Nonlinear Control **11**(5), 435–451 (2001)